PERGAMON

International Journal of Solids and Structures 37 (2000) 4737–4762

INTERNATIONAL JOURNAL OF SOLIDS and STRUCTURES

www.elsevier.com/locate/ijsolstr

The order of stress singularity near the vertex in three-dimensional joints

Hideo Koguchi[a,*], Takashi Muramoto[b]

[a]*Department of Mechanical Engineering, Nagaoka University of Technology, Kamitomioka 1603-1, Nagaoka, Niigata, 940-2188, Japan*

[b]*Department of Mechanical Engineering, Graduate School of Nagaoka University of Technology, Kamitomioka 1603-1, Nagaoka, Niigata, 940-2188, Japan*

Received 21 April 1998; in revised form 15 May 1999

Abstract

Dissimilar materials are frequently used in industrial products, such as electronic devices, welded joints and composite materials. Many investigations on two-dimensional joints so far have been carried out theoretically and experimentally, although three-dimensional ones are rarely performed. In this paper, the order of stress singularity at the corner where four free surfaces and the interfaces of the three-dimensional joints meet is investigated by solving an eigenequation derived from a finite element formulation. The order of stress singularity for four typical joints, referred to as the 1/8–1/8, 1/8–1/4, 1/8–1/2 joints and a joint with various vertex angles, consisting of two blocks with different properties is investigated. Dundurs' composite parameters, α_{3D} and β_{3D}, for three-dimensional joints are newly introduced, and the order of stress singularity plotted on ordinary Dundurs' parameters, the α and β plane, is rearranged on the α_{3D}–β_{3D} plane. The order of stress singularity at the vertex in the three-dimensional joints is larger than that in the two-dimensional joints, although, the zero boundary of stress singularity varies little on the α_{3D}–β_{3D} plane. Furthermore, it was shown that the order of stress singularity at a vertex, where some singular lines with different orders meet, varies with the combination of material properties.

Keywords: Three-dimensional joints; Stress singularity; Dundurs' parameters; Eigenequation; FEM

1. Introduction

Many investigations have been conducted so far concerning joints fabricated from materials with

* Corresponding author. Fax: +81-258-47-9770.
E-mail address: koguchi@mech.nagaokaut.ac.jp (H. Koguchi).

0020-7683/00/$ - see front matter
PII: S0020-7683(99)00159-6

different properties, in order to effectively utilize the feature of each material. Joint structures of bonded metals and ceramics have been used widely in electric devices and mechanical parts. It is known from previous studies that failure occurs and the reliability of the materials decreases due to the occurrence of stress singularity at the cross-point of the free surface and the bonded plane. There are many pre-existing cracks in ceramics, and in fact, fracture and delamination occur often around the vertex of joints. Such problems cause the decrease of reliability of joints. Therefore, many studies on the reduction of stress singularity have been carried out theoretically and experimentally (Koguchi et al., 1994). Almost all these studies are focused on two-dimensional stress singularity (Barsoum, 1988; Bogy, 1971a,b; Cook and Erdogan, 1972; Dempsey and Sinclair, 1979; Fenner, 1976; Hein and Erdogan, 1971; Koguchi et al., 1995; Theocaris, 1974; Yang and Munz, 1994). There is no evidence that these results are applicable to three-dimensional joints. In a practical point of view of fracture mechanics and an application of joints, an analysis of three-dimensional singularities would be very useful.

There are several investigations on the stress singularity field in three-dimensional elastic materials. Bazant (1974) first developed a general numerical procedure for determining three-dimensional stress singularities. Bazant and Kerr (1974) showed that a rigid conical inclusion induces much stronger concentration at its vertex than a conical notch of the same size. Kerr and Parihar (1977, 1978) investigated the three-dimensional stress concentrations at corners of stamps and pyramidal notches in isotropic materials. Benthem (1977, 1980) examined the singularity exponent of the stress field at the corner point of the free surface with a crack front in a three-dimensional crack. Bazant and Estenssoro (1979) extended the same method to determine the order of stress singularities for the previous study by Benthem. Somaratna and Ting (1986) extended the finite element scheme developed by Bazant and Estenssoro (1979) to incorporate general anisotropic elastic materials, and they investigated the order of stress singularity in laminated composite materials. Several important investigations regarding the accuracy of the method were made by Ghahremani (1991), Ghahremani and Shih (1992). Nakamura and Parks (1988) investigated the three-dimensional stress state at the vicinity of a through-crack front of an isotropic plate using a finite element method (FEM), and examined the corner stress intensity factor and the dependence of stress singularity on Poisson's ratio near the intersection of the crack front and free surface.

The stress field with singularities is readily accommodated in brittle solids by defects or pre-existing cracks. It is recognized that the stress concentration at grain triple junctions induced by thermal and elastic anisotropies of the grains plays a major role in crack nucleation. Ghahremani *et al.* (1990) analyzed the elastic anisotropy-induced stress concentrations at triple junctions in three dimensions, and showed that the concentration effect in three-dimensions to be stronger than those obtained for plane strain configurations. Picu and Gupta (1997) studies the stress singularity at the point of intersection of a grain triple junction line with the free surface in single-phase polycrystals of cubic and hexagonal grains using the special finite element method developed by Bazant (1974). They showed that the singularity exponents obtained were somewhat different and stronger in comparison with those obtained for the corresponding two-dimensional plane stress and strain configurations.

Pageau and Biggers (1995) extended the FEM formulation developed by Yamada and Okumura (1981) extended to account for anisotropy of materials. They investigated the three-dimensional intersection of multi-material junction with a free surface by using the FEM formulation (Pageau et al., 1994). They examined the influence of the numbers of mesh division and of Gauss integration points upon the accuracy of calculation. We performed analyses of three-dimensional joints using boundary element method (BEM) and showed that the order of stress singularity at a vertex of three-dimensional joints is stronger than that at a vertex of two-dimensional joints (Koguchi 1997; Li et al., 1992).

In contrast to these studies, relatively less attention has been given to the area of stress singularities in bonded structure with a general configuration. For example, a three-dimensional assembly of dissimilar isotropic materials with several vertices is shown in Fig. 1. In the case of three-dimensional joints, the

stress singularity occurs not only at the vertex but also along the intersection of the interface with the free surface. We refer to this as the stress singularity line. The vertex of three-dimensional joints is generally a cross-point of stress singularity lines with different exponents of stress singularity.

We showed in the previous paper (Koguchi, 1997) that the stress field around such a vertex consisted of several free surfaces and an interface can be expressed as a power law with respect to r, the distance from the vertex. Generally, the field for a stress component, σ_{kl}, near the vertex can be expressed, as follows:

In the case of real number of the order of stress singularity,

$$\sigma_{kl} = \sum_{j=1} r^{\lambda_j} F^{\ j}_{kl}(\phi, \theta, \lambda_j) \tag{1}$$

where ϕ and θ are angles in the spherical coordinates, F^j_{kl} are a function of angles ϕ, θ and the jth order of singularity.

In the case of complex number and real number of the order of stress singularity,

$$\sigma_{kl} = \sum_{j=1} r^{\lambda_j^{\mathrm{R}}} \{F^{*j\mathrm{R}}_{kl}(\phi, \theta, \lambda^*_j) \cos(\boldsymbol{\lambda}^{\mathrm{I}}_{\boldsymbol{j}} \ \ln \ r) - F^{*j\mathrm{I}}_{kl}(\phi, \theta, \lambda^*_j) \sin(\boldsymbol{\lambda}^{\mathrm{I}}_{\boldsymbol{j}} \ \ln \ r)\} + \sum_{j=1} r^{\lambda_j} F^{\ j}_{kl}(\phi, \theta, \lambda_j) \tag{2}$$

where $\lambda^*_j = \lambda^{\mathrm{R}}_j + i\lambda^{\mathrm{I}}_j$, $F^{*j}_{kl} = F^{*j\mathrm{R}}_{kl} + iF^{*j\mathrm{I}}_{kl}$ is a complex function of angles ϕ and θ and of the order of singularity. When $-1 < \lambda_1 < \lambda_2 < \ \ldots \ < 0$ or $-1 < Re(\lambda^*_1) < Re(\lambda^*_2) < \ \ldots \ < 0$, the stress field has a stress singularity, and when $\lambda_j > 0$ or $Re(\lambda^*_j)$, the stress singularity disappears.

When we estimate the strength and reliability of joints, we have to know the order of stress singularity and the functions, F^j_{kl} or F^{*j}_{kl}. The stress distribution around the vertex with singularity can be calculated using BEM and FEM. However, when a joint is made of materials yielding a complex number or several real numbers of the order of singularity, it is difficult to estimate the orders of stress

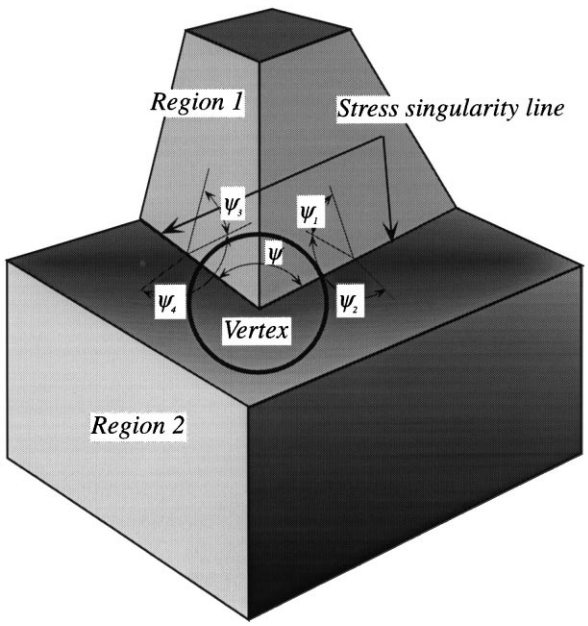

Fig. 1. Stress singularity lines and vertex at the intersection of side free-surfaces with interface in a three-dimensional joint.

singularity from the stress distribution. Once we know every value of the order of stress singularity, we can estimate a stress intensity factor at the vertex of the joint from the stress distribution obtained by FEM or BEM, taking the stress singularity into consideration in an interpolation function. Furthermore, when the order of stress singularity is arranged on Dundurs' parameters plane, it is very useful to estimate the stress intensity factor for various combinations of materials. Hence, we will examine the order of stress singularity for several configurations of joints. In this study, the order of stress singularity at a vertex in a rectangular parallelepiped joint is first investigated and then plotted on Dundurs' parameters plane (Dundurs, 1969) which is deduced in a three-dimensional stress state. Graphed results on the planes of Dundurs' parameters for a two-dimensional stress state and those for a three-dimensional are compared. As a consequence, we will show that the order of singularity in three-dimensional joints is related with elastic moduli of both materials in a rather complicated way. Here, the stress distributions for joints with several fixed angles between two free side surfaces, examined in the previous paper using BEM, are also investigated using FEM. Finally, we examined a rectangular parallelepiped block bonded to another block in the cases where one block is displaced on the bonded plane in the x-direction or x-, y-direction. In this situation, the problem can be simplified by restricting the vertex such that a 1/8-elastic region is bonded to a half-infinite elastic region and a quarter-infinite region, respectively. These models correspond to the stress singularity at the corner where an electronic IC is bonded to a base plate.

2. Dundurs' parameters for two- and three-dimensional stress state

Dundurs introduced the well-known parameters (Dundurs, 1969), α–β, utilizing a description of a stress state in two-dimensional dissimilar materials in the discussion of Bogy's paper. We will later derive the Dundurs' parameters for three-dimensional dissimilar materials, so we will refer to it as α_{2D}–β_{2D} adding the subscript 2D to the original Dundurs' parameters. Dundurs' parameters, α_{2D}–β_{2D}, for two-dimensional dissimilar materials can be expressed using pairs of material properties (G, ν)

$$\alpha_{2D} = \frac{m_2 - m_1\Gamma}{m_2 + m_1\Gamma}$$

$$\beta_{2D} = \frac{(m_2 - 2) - (m_1 - 2)\Gamma}{m_2 + m_1\Gamma} \tag{3}$$

where

$$\Gamma = \frac{G_2}{G_1} \tag{4}$$

$$m_i = \begin{cases} 4(1-\nu_i) & \text{for plane strain} \\ \dfrac{4}{1+\nu_i} & \text{for plane stress} \end{cases} \qquad (i = 1, 2) \tag{5}$$

in which G is the shear modulus and ν is Poisson's ratio. The subscripts of these material properties represent the region of materials; 1 refers to the upper region and 2 the lower region in Fig. 1.

Here, since the mechanical properties for all materials are in the range of $G_1, G_2 \geq 0$, $0 \leq \nu_1, \nu_2 \leq 0.5$, the existence domain of α_{2D} and β_{2D} for two-dimensional stress states is within the boundary enclosed by four straight lines, as follows

$$\alpha_{2D} = \pm 1$$

$$\beta_{2D} = \begin{cases} \dfrac{\alpha_{2D} \pm 1}{4} & \text{for plane strain} \\ \dfrac{3\alpha_{2D} \pm 1}{8} & \text{for plane stress} \end{cases}. \tag{6}$$

The order of stress singularity in two-dimensional joints and the condition of the disappearance of stress singularity can be represented on the plane of Dundurs' parameters (Bogy, 1968; 1970; 1971a,b). The order of stress singularity for two-dimensional dissimilar materials could also be represented consistently on Dundurs' plane regardless of different combinations of Poisson's ratios and elastic moduli.

As previously mentioned, the region of Dundurs' parameters defined for plane stress differs from that for plane strain in two-dimensional joints. Generally, the stress states in three-dimensional joints are between plane stress and plane strain, and hence, it may not be possible to simply arrange the order of stress singularity on the plane of Dundurs' parameters α_{2D}–β_{2D}. Therefore, Dundurs' parameters for a three-dimensional stress state are deduced. Hooke's law for three-dimensional elasticity can be expressed as

$$\epsilon_{ij} = \frac{1}{2G}(\sigma_{ij} - \nu'\sigma_{kk}\delta_{ij}) \quad (i, j = 1, 2, 3), \tag{7}$$

where ϵ_{ij} represents a strain component, σ_{ij} a stress component, Einstein's summation convention is used, G is transverse elastic modulus, and

$$\nu' = \frac{\nu}{1+\nu}. \tag{8}$$

First, three components of normal stress in Eq. (7) are equated with each other assuming an isotropic stress state.

$$\epsilon_{kk} = \frac{1-3\nu'}{2G}\sigma_{kk} = A\sigma_{kk}, \tag{9}$$

where A is referred to as volumetric compliance.

Next, the normal stress components are taken as $\sigma_{22} = \sigma_{33} = 0$ considering a uniaxial stress state

$$\epsilon_{11} = \frac{1-\nu'}{2G}\sigma_{11} = C\sigma_{11} \tag{10}$$

where C is referred to as uniaxial compliance.

Dundurs' parameters, α_{3D} and β_{3D}, for a three-dimensional stress state can be represented by following the definition of Dundurs' parameters, α_{2D} and β_{2D}

$$\alpha_{3D} = \frac{C_1 - C_2}{C_1 + C_2} = \frac{\Gamma(1-\nu_{1,}') - (1-\nu_2')}{\Gamma(1-\nu_{1,}') + (1-\nu_2')} \tag{11}$$

$$\beta_{3D} = \frac{A_1 - A_2}{C_1 + C_2} = \frac{\Gamma(1-3\nu_1') - (1-3\nu_2')}{\Gamma(1-\nu_{1,}') + (1-\nu_2')}, \tag{12}$$

where

$$A_i = \frac{1-3\nu_i'}{2G_i}, \quad C_i = \frac{1-\nu_i'}{2G_i} \quad (i=1,2) \tag{13}$$

$$\nu_i' = \frac{\nu_i}{1+\nu_i} \quad (i=1,2). \tag{14}$$

The α_{3D}–β_{3D} plane is the domain enclosed by the following four lines, and is shown in Fig. 2

$$\alpha_{3D} = \pm 1, \quad \beta_{3D} = \frac{\alpha_{3D} \pm 1}{2}. \tag{15}$$

This domain is expanded in the β_{3D}-direction in comparison with the plane of two-dimensional parameters.

3. Method and model for analysis

3.1. Method for analysis

In the previous paper (Koguchi, 1997), the stress field near the vertex of three-dimensional joints was analyzed by varying several angles of the free surfaces intersecting the interface. BEM specially developed using Rongved's fundamental solutions (Rongved, 1955) for two-phase materials was used in that analysis. It was shown that the stress field near the vertex could be expressed by a power-law of the order of stress singularity. When conventional BEM and FEM are used in a stress analysis, the stress distributions only under a certain condition are calculated. In this case, it is difficult for the order of singularity to be estimated from the stress distribution. Furthermore, a vast memory is required for accurately analyzing the stress fields. It is important for estimating the reliability of real bonded structures to clarify the difference between the order of stress singularity in two-dimensional joints and that in three-dimensional joints. It is noted that the number of roots yielding a stress singularity in an eigenequation derived later from the principle of virtual work is occasionally more than two. In such a case, each root is hard to be distinguished from the other in the stress distribution.

In this paper, FEM formulation using an interpolation function of displacements, considering the

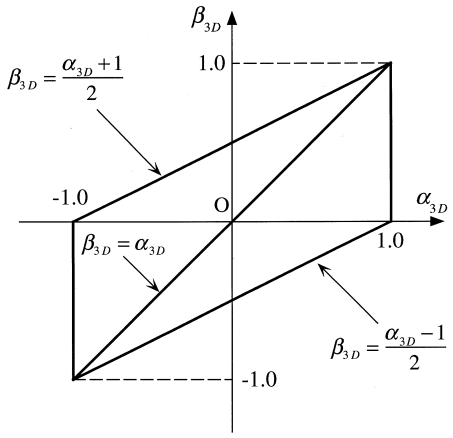

Fig. 2. Plane of three-dimensional Dundurs' parameters, α_{3D}–β_{3D}.

stress singularity presented by Yamada and Okumura (1981) and Pageau and Biggers (1995) is used to analyze the order of stress singularity. We can obtain multiple real and complex roots as eigenvalues for the eigenequation of the displacement vector, and examine the order of stress singularity. We will describe briefly the derivation of the eigenequation. Body forces are not taken into account in our analysis. A spherical domain with the origin at the vertex with the stress singularity is divided into finite elements, as shown in Fig. 3. The distance, r, from the origin O to an inner point Q of the sphere is expressed as

$$r = \rho r_0 = r_0 \left(\frac{1+\zeta}{2} \right)^p, \tag{16}$$

where p is an unknown characteristic value governing the stress field, r_0 represents a radius of the spherical domain, and $-1 < \zeta < 1$.

Taking the displacement at the origin as zero, the discretized displacement vector, $\mathbf{u}_i$, at nodes can be expressed as

$$\mathbf{u}_i = \rho^p \left[\sum_{j=1}^{8} H_j u_{ij} \right], \tag{17}$$

where H_j represents the serendipity quadratic interpolation function, and u_{ij} is the i-component of displacement at node j.

The strain for the element is expressed using the equation of displacement, and also angles θ and ϕ for spherical coordinates are expressed using the interpolation function as follows:

$$\theta = \sum_{j=1}^{8} H_j \theta_j, \quad \phi = \sum_{j=1}^{8} H_j \phi_j. \tag{18}$$

The following is the eigenequation derived by the principles of virtual work for calculating the

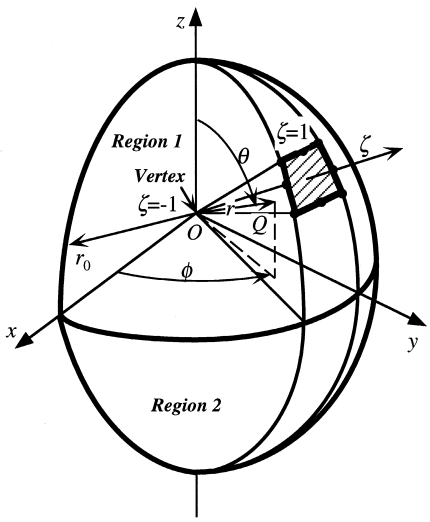

Fig. 3. Finite element geometry and coordinate systems with the origin at the vertex of joints.

eigenvalue, p

$$(p^2[A] + p[B] + [C])\{U\} = 0. \tag{19}$$

Finally, the eigenequation is modified into a generalized eigenequation, and the eigenvalues, p, are deduced by solving the equation. One refers to other papers for details (Pageau and Biggers, 1995; Yamada and Okumura, 1981).

In order to check the validity of the developed program, the order of singularity in a three-dimensional crack, where the front line intersects perpendicularly with a free surface, was numerically derived. The same problem was analyzed theoretically by Benthem (1977, 1980), who showed that the order of singularity varies with Poisson's ratio. The domain for analysis is semispherical, and a three-dimensional crack exists on the plane of $\phi = 0$ degree as shown in Fig. 4(a) and mesh division used in this analysis is shown in Fig. 4(b) and (c). The relationship between the order of singularity and Poisson's ratio is shown in Fig. 5. Analysis was performed by varying the mesh size as $\phi \times \theta = 30^\circ \times 30^\circ$ and $45^\circ \times 45^\circ$, which means that the domain for analysis is divided into twelve and eight, respectively, in the ϕ-direction, and three and two, respectively, in the θ-direction. The maximum error in a finer mesh division is less than 2% in comparison with Benthem's result.

Furthermore, we will examine the influence of mesh size and of the number of integration points of Gauss integration upon the numerical values of order of stress singularity in a joint. A model for analysis is the joint referred to as model 1 shown in Fig. 6. This model was used in the previous paper (Koguchi, 1997) and the order of singularity for the model was investigated using BEM. Mechanical properties of the joint used in the analysis were described as follows. Young's moduli of material 1 and 2 are 100 GPa and 500 GPa, and Poisson's ratios are 0.37 and 0.25, respectively. The order of stress singularity estimated from the slope of plotted line of stress distribution in a log-log scale was -0.208, which obtained by applying least square method for the stress distribution in $r/L < 6.5 \times 10^{-5}$. Here, the width of joint is adapted as L ($=10$ mm). The order of stress singularity obtained in the present numerical method is shown in Figs. 7 and 8. Fig. 7 represents the variation of the order of singularity with the number of integration points. In the analysis, the mesh size is fixed as $\phi \times \theta = 22.5^\circ \times 22.5^\circ$. The value of order of singularity increases from -0.27069 to -0.2076 with increasing the number of integration points. The error of FEM against BEM is less than 0.2%. Fig. 8 shows the variation of the order of singularity with decrease of angle of an element. The order of singularity increases up to -0.2081 with decreasing the mesh size. We can say that the results of FEM are fairly agreed with that of BEM. In the model 1, the singular field with the order of -0.208 is dominant within $r/L < 6.5 \times 10^{-5}$. FEM formulation used here is useful for calculating easily the order of singularity by solving the eigenequation.

3.2. Models of three-dimensional analysis

Fig. 6 shown before represents models for joints used in the analysis. Model 1 is the joint of the reference configuration and of angles $\psi_1 = \psi_2 = \psi_3 = \psi_4 = \psi = 90^\circ$ (see Fig. 1). A joint varied with a vertex angle between two free side surfaces holding the relationship of $\psi_1 = \psi_2 = \psi_3 = \psi_4 = 90^\circ$ is referred to as model 2. The joints of the same configurations, models 1 and 2, were used in the previous paper, but the order of singularity was not examined precisely for various combinations of material properties. In this paper, the planes of α_{2D}–β_{2D} and α_{3D}–β_{3D} are constructed by conducting the analysis for many combinations of materials and compared with each other. Joints, which a rectangular parallelepiped block is bonded with the quarter (model 3) and the half (model 4) regions with different mechanical properties, are furthermore investigated. The results for three-dimensional joints are compared with the results for two-dimensional joints, which have the same cross section as three-dimensional joints.

Furthermore, when two rectangular parallelepiped blocks are bonded to each other, it is difficult to accurately adjust the free side surfaces. These models demonstrate the situation where the block moves in a parallel direction to their interfaces. Several roots exhibiting the stress singularity occur in models 3 and 4, and hence the number of roots and their values are investigated for the ratio of Young's modulus of materials.

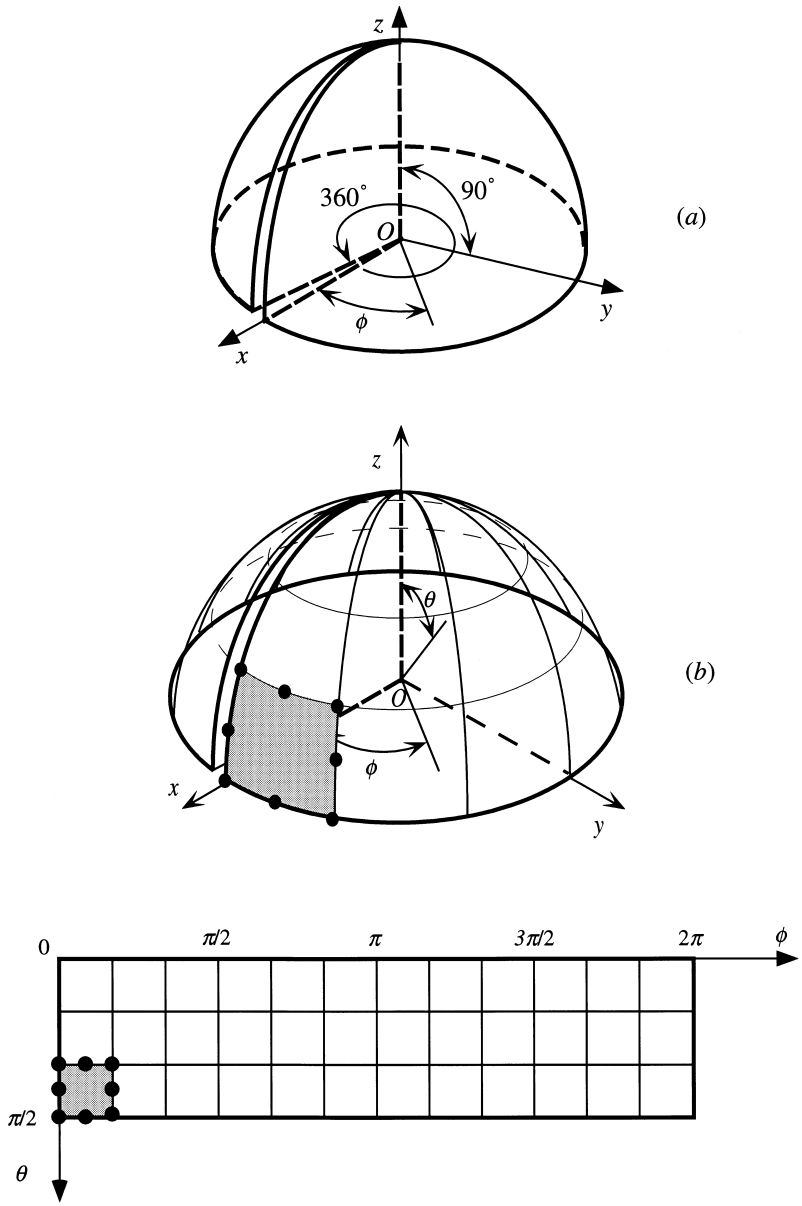

Fig. 4. A three-dimensional crack in a half-infinite elastic region. (a) Coordinate systems in the analysis, (b) mesh division of region for analysis, and (c) mesh division on θ–ϕ coordinates system.

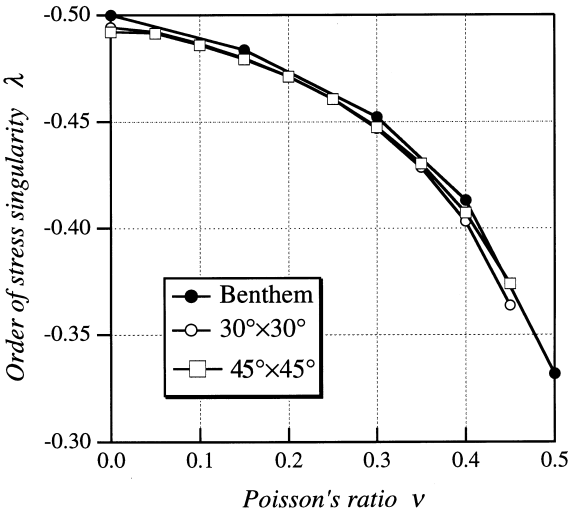

Fig. 5. The relationship between the order of stress singularity and Poisson's ratio.

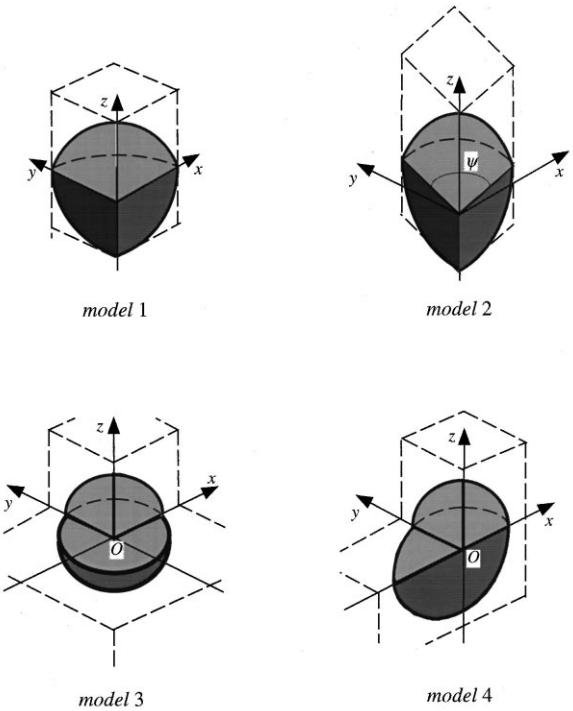

Fig. 6. Configuration of joints for analyses. Model 1 ($\psi_1=\psi_2=\psi_3=\psi_4=\psi=90^\circ$), model 2 ($\psi_1=\psi_2=\psi_3=\psi_4=90^\circ$, and ψ is variable), model 3 ($\psi_1=\psi_3=\psi=90^\circ$, $\psi_2=\psi 4=180^\circ$) and model 4 ($\psi_1=\psi_2=\psi_3=\psi=90^\circ$, and $\psi_4=180^\circ$).

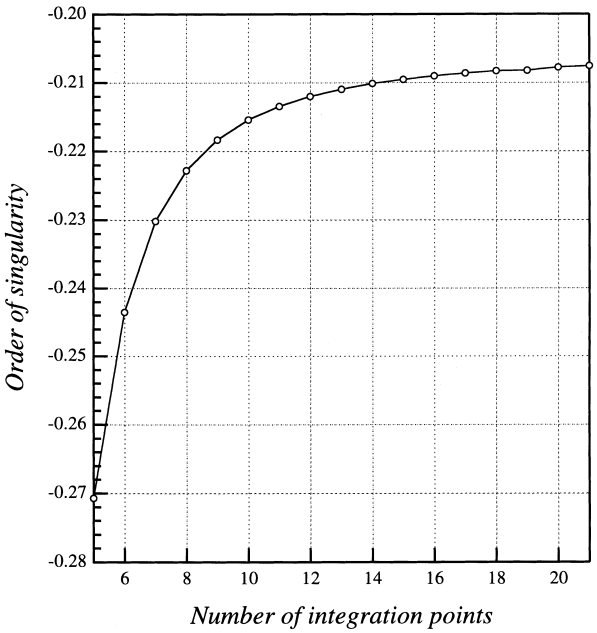

Fig. 7. Convergence of l for model 1 against the number of Gauss integration points.

3.3. Procedure for analysis

Many combinations of materials yielding the same value of Dundurs' parameters generally exist. However, the material properties used in the numerical analysis need to be determined in order to appropriately map the contour of the order of stress singularity. Hence, Young's modulus and Poisson's ratio, E_1 and ν_1, of material 1 are fixed, then E_2 and ν_2 of material 2 are determined for the given

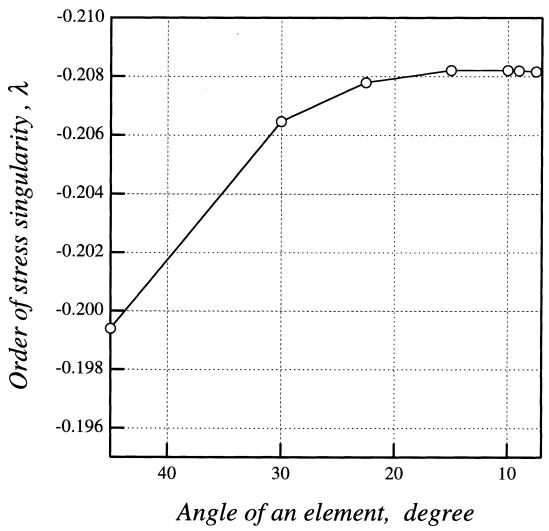

Fig. 8. Variation of the order of stress singularity with decrease of angle of an element.

Dundurs' parameters, α_{2D} and β_{2D}, by

$$E_2 = \frac{2G_1(1+\nu_2)}{\kappa} \tag{20}$$

$$\nu_2 = \begin{cases} 1 - \dfrac{m_2}{4} & \text{for plane strain} \\ \dfrac{4}{m_2} - 1 & \text{for plane stress} \end{cases}, \tag{21}$$

where

$$G_1 = \frac{E_1}{2(1+\nu_1)} \tag{22}$$

$$\kappa = \frac{1 - \alpha_{2D} + \alpha_{2D} m_1 - \beta_{2D} m_1}{1 - \alpha_{2D}} \tag{23}$$

$$m_2 = \frac{m_1(\alpha_{2D}+1)}{1 - \alpha_{2D} + \alpha_{2D} m_1 - \beta_{2D} m_1}. \tag{24}$$

Here, the Dundurs' parameters for two-dimensional stress states are employed to compare the contour map of the order of stress singularity for two-dimensional joints and three-dimensional joints. When material properties are determined using α_{2D} and β_{2D}, it is noted that unusual values of material properties, $\nu_2 < 0$, $\nu_2 > 0.5$ and $G_2 < 0$, are sometimes obtained. So, the range of α_{2D}–β_{2D} employed for analysis is determined by Poisson's ratio of material 1 in this case. Hence, we carry out analyses for several values of ν_1.

4. Results and discussion

4.1. The contour map of the order of stress singularity in model 1

Mesh division for model 1 is shown in Fig. 9. This model is composed of two 1/8-spheres with different properties. Mechanical properties for material 1 in the analysis were fixed at 206.0 GPa for E_1 and 0.1, 0.2, 0.3, 0.4 for ν_1. Then, E_2 and ν_2 were determined by using Eqs. (20)–(24), which can apply to any value of α_{2D} and β_{2D}.

The order of stress singularity in two-dimensional joints with rectangular vertex angles was examined by a two-dimensional FEM formulated in the same manner as the three-dimensional FEM. The zero-boundary of singularity in two-dimensional joints for model 1 is represented by two lines, $\alpha_{2D} = 0$ and $\beta_{2D} = \alpha_{2D}/2$, regardless of Poisson's ratio. In this study, the zero-boundary of singularity in three-dimensional joints was examined precisely in the regions $\beta \leq 0$ near $\alpha_{2D} = 0$ and $\alpha_{2D} \geq 0$ near $\beta_{2D} = \alpha_{2D}/2$. For instance, the point yielding the exact value for zero-singularity in three-dimensional joints was examined by varying the value of α_{2D} while holding β_{2D} at a fixed value. Furthermore, the loci of the root of characteristic equations for the order of stress singularity, 0.9, 0.8, and so on, are investigated in the same manner locating the zero-boundary of stress singularity. This procedure was repeated until the order of stress singularity agreed with a fixed value out to three digits. Fig. 10 shows the loci of the fixed order of stress singularity for Poisson's ratio, $\nu_1 = 0.4$, in two- and three-dimensional joints on the

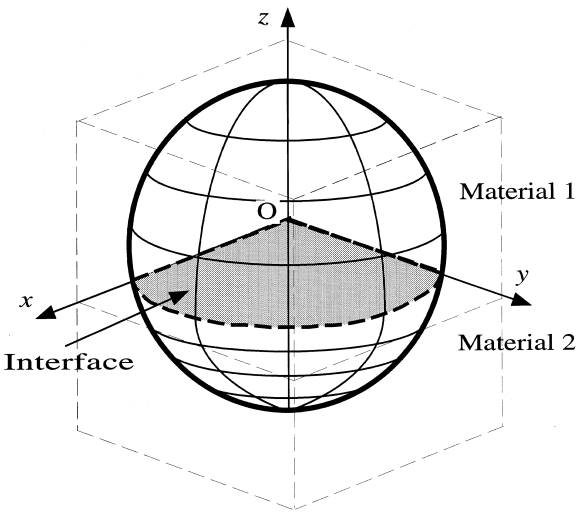

Fig. 9. Typical model of joint of model 1 and mesh division.

α_{2D}–β_{2D} plane. It is representative of the loci of the other Poisson's ratio which are similar to each other. The bold solid line, $\beta_{2D}=\alpha_{2D}/2$, shows the zero-boundary of singularity in two-dimensional joints. The results (open symbols) plotted in this figure show the order of two-dimensional joints obtained by FEM. When the loci of a two-dimensional analysis are compared with those of a three-dimensional analysis with the same value of order, for instance $\lambda=-0.3$, the loci of three-dimensional joints appear on a curve above the loci of two-dimensional joints. This indicates that a higher

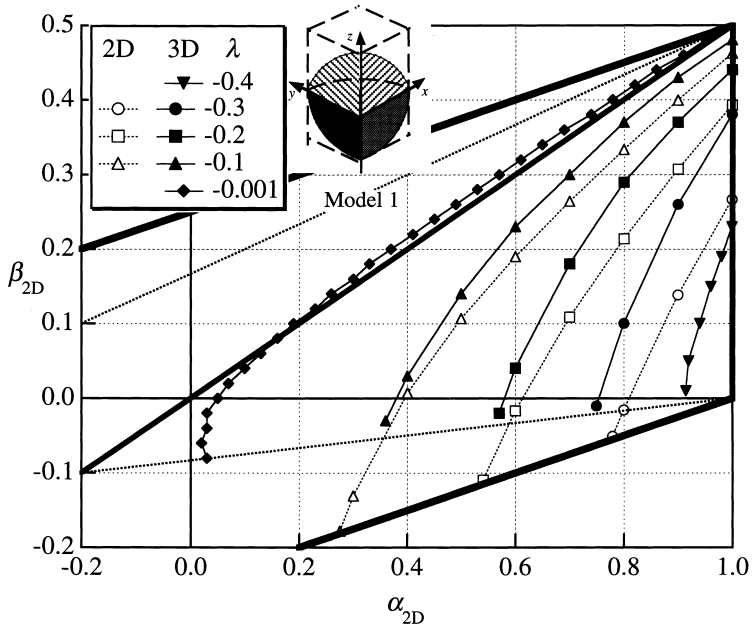

Fig. 10. The loci on the α_{2D}–β_{2D} plane of the order of stress singularity for two- and three-dimensional joints.

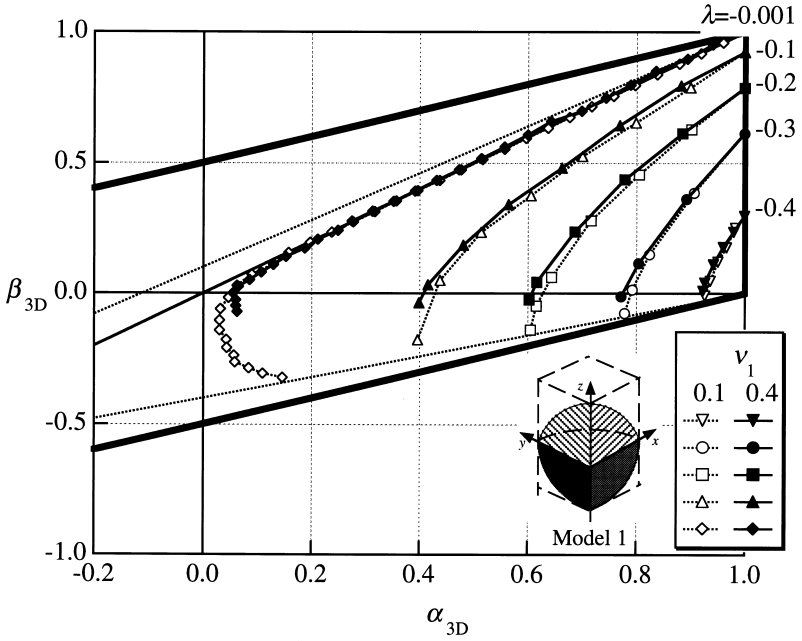

Fig. 11. The loci on the α_{3D}–β_{3D} plane of the order of stress singularity in three-dimensional joints for various Poisson's ratios of material 1.

singularity occurs in three-dimensional joints than in two-dimensional joints, when the combinations of material properties have the same (α_{2D}, β_{2D}). Furthermore, we can see from this figure that the zero-boundary of singularity in three-dimensional joints is not very different from that in two-dimensional joints.

Dependency of Poisson's ratio of the order of singularity is examined for various Poisson's ratios, and the loci of order of singularity on the α_{3D}–β_{3D} plane for $\nu_1 = 0.1$ and 0.4 are both shown in Fig. 11. It is found that the dependency of Poisson's ratio is fairly small on the α_{3D}–β_{3D} plane and disappears near $\beta_{3D} = \alpha_{3D}$. It is suggested from Fig. 11 that the zero-boundary of singularity exits on the lines $\beta_{3D} = \alpha_{3D}$ and near $\alpha_{3D} = 0.0$, which corresponds to the zero-boundary for two-dimensional joints. The zero-boundaries of singularity for $\nu_1 = 0.4$ and 0.1 are identical, although the loci for the same order of singularity shifts more to the right in $\nu_1 = 0.1$ than in $\nu_1 = 0.4$. More precise studies are necessary to determine the dependency of Poisson's ratio near $\alpha_{3D} = 0.0$. The zero-boundary of singularity on $\beta_{3D} = \alpha_{3D}$ does not vary with Poisson's ratio, conversely the zero-boundary of singularity near $\alpha_{3D} = 0.0$ is more likely to move with Poisson's ratio.

4.2. The contour plot of the order of stress singularity in model 2

In the previous paper (Koguchi, 1997), we examined the influence of varying the angle of ψ (see Fig. 1) on the order of singularity at the vertex between two free side surfaces in three-dimensional joints. First, the variation of the order of singularity with the angle ψ, namely, the order of singularity for joints with the angles, $\psi = 45°$, 60°, 90°, 120° and 150° holding the angles of $\psi_1 = \psi_2 = \psi_3 = \psi_4 = 90°$ is investigated and compared with the results obtained by BEM (Koguchi, 1997). The results of FEM and BEM are shown in Table 1. The values of BEM were obtained by approximating the stress distribution within $r/L < 10^{-3}$ using least square method. Where r is the distance from the vertex with singularity,

and L is a representative length of joint. Here, the width of joint is taken as $L(=10$ mm). FEM calculation was carried out under the condition that the number of integration points was 20 and the mesh size of element was $\phi \times \theta = 22.5^\circ \times 22.5^\circ$. The maximum error of results of FEM against BEM is about 2% at the apex angle of 60°. Fig. 12 shows the comparison of FEM and BEM for the relationship of the ratio of λ to $\lambda_{\text{plane stress}}$ against $\lambda_{\text{plane strain}}$. Solid symbols represent the results for BEM, which is already reported in the previous paper. Both results are agreed with each other.

Next, the variation of the order of singularity with the angle ψ, namely, the order of singularity for joints with the angles, $\psi = 22.5^\circ$, 45°, 67.5°, 90°, 112.5° and 135° holding the angles of $\psi_1 = \psi_2 = \psi_3 = \psi_4 = 90^\circ$ is investigated on the α_{3D}–β_{3D} plane. The angles of element per mesh division are ordinarily $\phi \times \theta = 22.5^\circ \times 22.5^\circ$. Furthermore, in order to investigate the effect of the angle of element on the order of singularity, an analysis for the angle of element being half that of the ordinary angle was performed, since the decrease of the vertex angle, ψ, causes the reduction of the number of elements. The numbers of elements and mesh divisions used in the analyses are shown in Table 2. Young's modulus and Poisson's ratio for material 1 were taken as $E_1 = 206.0$ GPa and $\nu_1 = 0.3$, respectively. Mechanical properties for material 2 were determined as mentioned previously.

The loci on the α_{2D}–β_{2D} plane for the joints with vertex angles ψ smaller than 90° are presented in Fig. 13. The loci of order of singularity shifts to the left as the vertex angle ψ decreases. This suggests that the order of singularity becomes larger when the angle ψ decreases. The larger values of the order of singularity, e.g. the loci for $\lambda = -0.4$ and -0.3, shift more than those for a smaller value, e.g. $\lambda = -0.1$, with the variation of the angle ψ. The loci for the angles $\psi = 22.5^\circ$ and 45° show that there is only a slight influence on the order of singularity by these values of the angle ψ. But, the influence of the angle ψ becomes obvious over $\psi = 45^\circ$. The zero-boundary of singularity on $\beta_{2D} = \alpha_{2D}/2$ shifts very slightly, even if the vertex angle ψ varies, although the zero-boundary near $\alpha_{2D} = 0$ moves in the direction of a negative value of α with the decreasing angle of ψ.

The loci of order of singularity in joints with the angle, $\psi = 22.5^\circ$, are shown in Fig. 14, where the analysis was performed employing a finer mesh division to examine the accuracy of the calculation. The difference of loci for $\phi \times \theta = 25^\circ \times 25^\circ$ and $12.5^\circ \times 12.5^\circ$ was very small, and dependency of the loci on the mesh division could not be found clearly in our calculation.

The loci of the order of singularity for the angles, $\psi = 90.0^\circ$, 112.5°, and 135.0°, are represented in Fig. 15, and each locus shifts slightly down to the right with the increasing angle of ψ. This suggests that the order of singularity decreases with the increasing angle of ψ. When the Dundurs' parameters

Table 1
A comparison of the order of singularity obtained from BEM and FEM for model 2

E_1	ν_1	E_2	ν_2		45°	60°	90°	120°	150°
100	0.15	27.5	0.422	FEM	0.191657	0.186849	0.175582	0.163493	0.152194
				BEM	0.18939	0.182546	0.176174	0.163666	0.151984
100	0.2	19.99	0.450	FEM	0.246698	0.24196	0.230637	0.217742	0.20465
				BEM	0.245938	0.239008	0.23100	0.218064	0.204974
100	0.3	14.26	0.475	FEM	0.298073	0.29407	0.284162	0.271855	0.25790
				BEM	0.298078	0.290972	0.284988	0.272085	0.25806
100	0.15	8.34	0.477	FEM	0.363256	0.357717	0.34456	0.329233	0.312431
				BEM	0.364056	0.355971	0.345114	0.330099	0.313005
100	0.1	3.96	0.488	FEM	0.420023	0.414556	0.401456	0.385623	0.36689
				BEM	0.42201	0.41202	0.40203	0.3861	0.36693

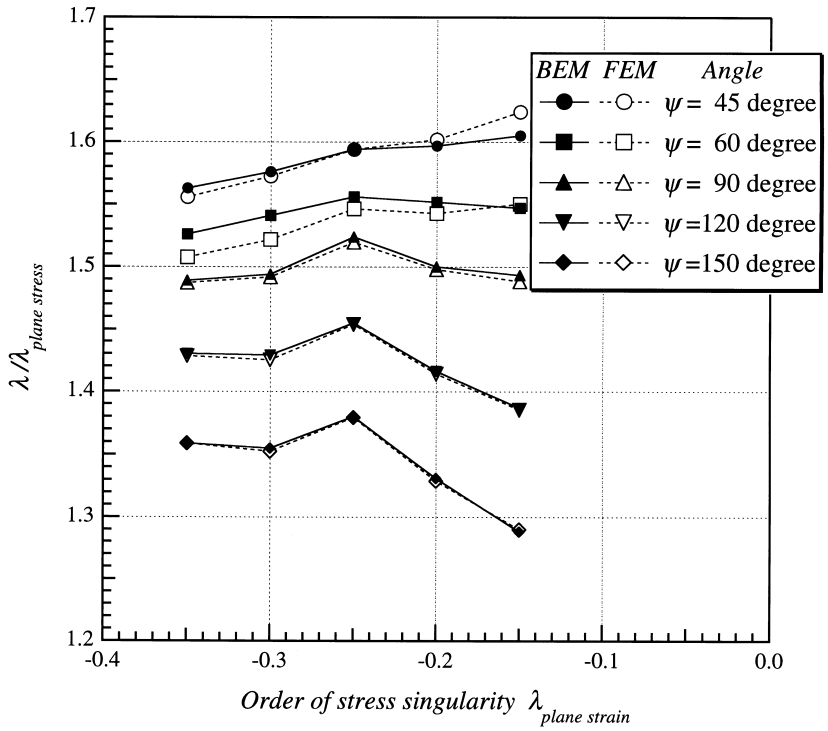

Fig. 12. A comparison of FEM and BEM for the relationship of the ratio of λ to $\lambda_{\text{plane stress}}$ against $\lambda_{\text{plane strain}}$.

(α_{2D}, β_{2D}) are fixed, the influence of the angle, ψ, on singularity becomes large when a combination of materials generating a large order of singularity is used.

The loci of the order of singularity for $\psi = 45^\circ$, 90°, and 135° are shown in Fig. 16. The loci on the α_{3D}–β_{3D} plane are similar to that on the α_{2D}–β_{2D} plane, i.e. they shift upwards to the left with the decreasing angle of ψ, and shift downwards to the right with the increasing angle of ψ. Comparing each locus for the same combination of materials, the order of singularity in a smaller vertex angle, ψ, is larger than that in a larger vertex angle ψ. Apparently, the locus for a material combination generating higher stress singularity shifts considerably. The zero-boundary of singularity on $\beta_{3D} = \alpha_{3D}$ moves slightly with the variation of the angle ψ, however, the zero-boundary of singularity near $\alpha_{3D} = 0$ shifts to $\alpha_{3D} = 1$ and -1 for the larger and smaller angles, ψ, than 90°, respectively.

Table 2
Number of elements and nodes

Vertex angle ψ	Number of elements	Number of nodes
22.5°	8 (32)	43 (133)
45.0°	16	69
67.5°	24	95
90.0°	32	121
112.5°	40	147
135.0°	48	173

4.3. Comparison of the order of stress singularity in models 1, 3 and 4

Models 3 and 4 (see Fig. 6) represent joints where one of the two blocks initially agreeing with every free side-surface is displaced on the bonded plane in the x-direction and the x-, y-directions, respectively. The 1/8–1/2 and 1/8–1/4 three-dimensional joints corresponding to the joints with edge angles $\pi/2$–$\pi/2$ and $\pi/2$–π in two-dimensional dissimilar materials are analyzed here. It is difficult to map the loci of the order of singularity for these joints on Dundurs' parameters plane, since plural roots yielding stress singularity usually occur in these joints. Hence, in this section, the order of singularity is examined against E_1/E_2, a ratio of rigidity of material 1 to material 2, by varying Poisson's ratio for material 2. Specifically, Young's modulus and Poisson's ratio of material 1 were fixed as $E_1 = 200.0$ GPa and $\nu_1 = 0.3$, respectively. Then, Poisson's ratio of material 2 was taken as 0.0, 0.1, 0.2, 0.3, 0.4 and 0.48, and Young's modulus of material 2 was determined using the method described in the previous section 3.3.

Fig. 17 shows an example of a mesh division for the 1/8–1/4 joint, where the size of an element is $\phi \times \theta = 22.5^\circ \times 22.5^\circ$, the number of elements is 48, and the number of nodes is 177. In the 1/8–1/8 joint, the same element size as in the 1/8–1/4 joint is used, and the numbers of elements and nodes are 32 and 121, respectively. In the 1/8–1/2 joint, the numbers of elements and nodes are 45 and 165, respectively.

The order of singularity of model 1 is demonstrated against E_1/E_2 for $\nu_2 = 0.0$, 0.3, and 0.48 in Fig. 18. The dashed line in the figures represents the order of singularity for two-dimensional joints with the edge angles, $\pi/2$–$\pi/2$. The figures show the variation of order along the line connecting a point on $\alpha_{2D} = -1$ with a point on $\alpha_{2D} = 1$ on Dundurs' parameters plane. The results for two- and three-dimensional joints for $\nu_2 = 0.0$ are shown in Fig. 6(a), where stress singularity occurs at $E_1/E_2 < 1.0$, and a stronger singularity is generated in three-dimensional joints than in two-dimensional joints. The order of singularity in two- and three-dimensional joints has a similar variation against E_1/E_2. With increasing

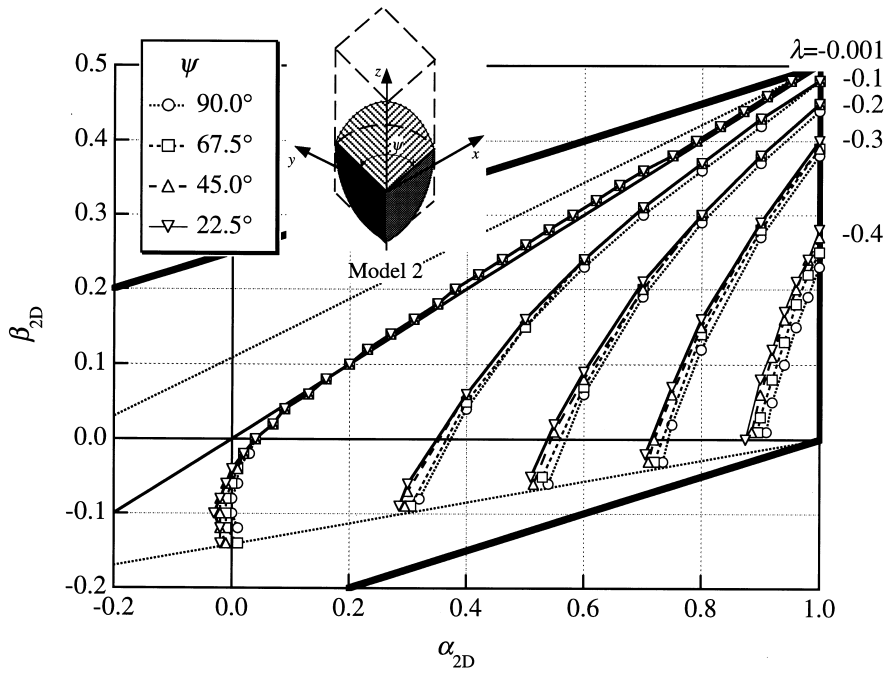

Fig. 13. The loci on the α_{2D}–β_{2D} plane of the order of stress singularity for the joints withvertex angles ψ smaller than 90°.

ν_2, stress singularity occurs also at $E_1/E_2 > 1.0$, and the variation of order against E_1/E_2 in three-dimensional joints is similar to that in two-dimensional joints. It is observed from these figures that the order of singularity for three-dimensional joints is 1.3 times larger than that for two-dimensional joints in the range of larger and smaller ratios of rigidity.

The order of singularity for model 3 is shown against E_1/E_2 for $\nu_2 = 0.0$, 0.3, and 0.48 in Fig. 19. Bold solid and dashed lines show real and imaginary values of the order of singularity for three-dimensional joints, respectively. The order of singularity for two-dimensional joints with the edge angles, $\pi/2$–π, is also represented by thin solid and thin dashed lines in this figure. In this joint, the order of singularity does not vary symmetrically with respect to $E_1/E_2 = 1$, even if ν_1 is equal to ν_2, since the apex angles of material 1 and 2 are different from each other.

When ν_2 is equal to 0.0, two roots generate the stress singularity in two-dimensional joints in $E_1/E_2 < 6$. As the value of E_1/E_2 increases, the two roots meet around $E_1/E_2 = 6$, and two complex roots, including a conjugate complex root, are generated at $E_1/E_2 > 6$. The order of singularity in three-dimensional joints varies against E_1/E_2 in a similar manner to two-dimensional joints. Three real roots exist in $E_1/E_2 < 30$ and two of them intersect around $E_1/E_2 = 30$. One real root and two complex roots, including a conjugate complex root, are generated at $E_1/E_2 > 30$.

With increasing Poisson's ratio of material 2, the transition point from two real roots to complex roots shifts to a larger value of E_1/E_2 and the imaginary values of their complex roots decrease in both joints. The imaginary value of the order of singularity tends to decrease more significantly in three-dimensional joints than in two-dimensional joints. In the case of $\nu_2 = 0.48$, three different values for the

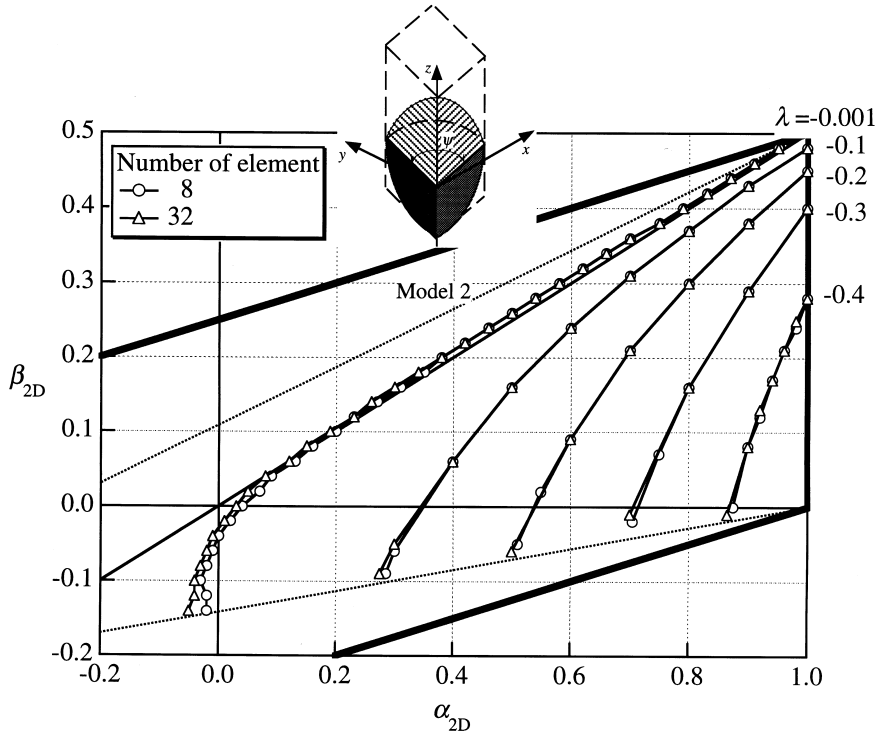

Fig. 14. The loci on the α_{2D}–β_{2D} plane of order of singularity in joints with the angle $\psi = 22.5°$ for different mesh divisions, $\phi \times \theta = 25° \times 25°$ and $12.5° \times 12.5°$.

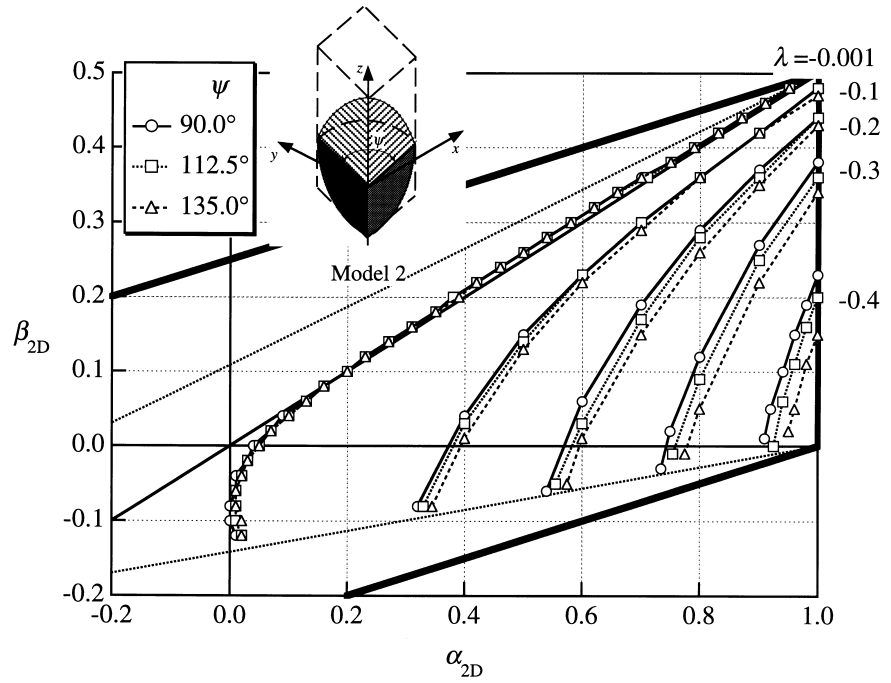

Fig. 15. The loci on the α_{2D}–β_{2D} plane of the order of singularity for the angles, $\psi = 90.0°$, 112.5°, and 135.0°.

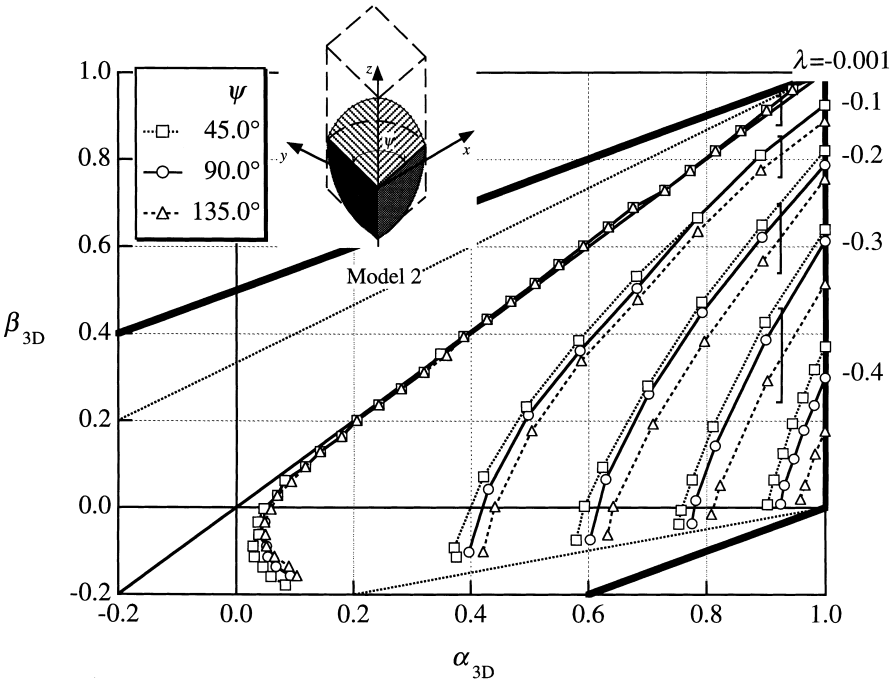

Fig. 16. The loci on the α_{3D}–β_{3D} plane of the order of singularity for $\psi = 45°$, 90°, and 135°.

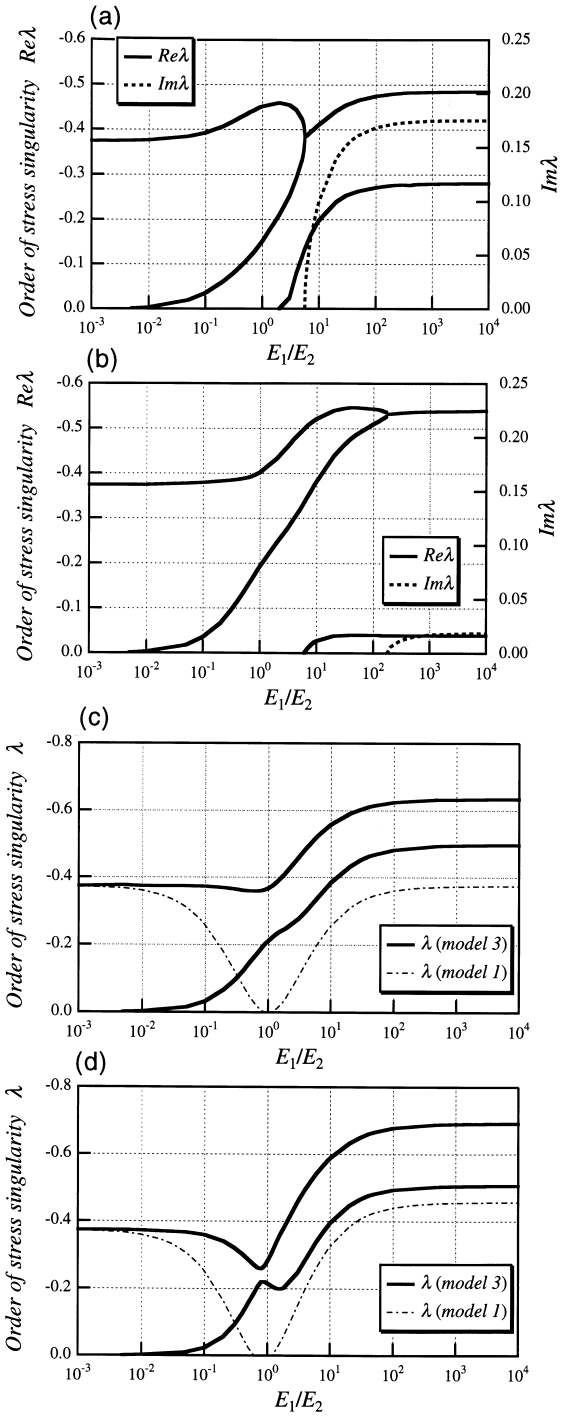

Fig. 17. An example of a mesh division for the 1/8–1/4 joint, where the size of element is $\phi \times \theta = 22.5^\circ \times 22.5^\circ$.

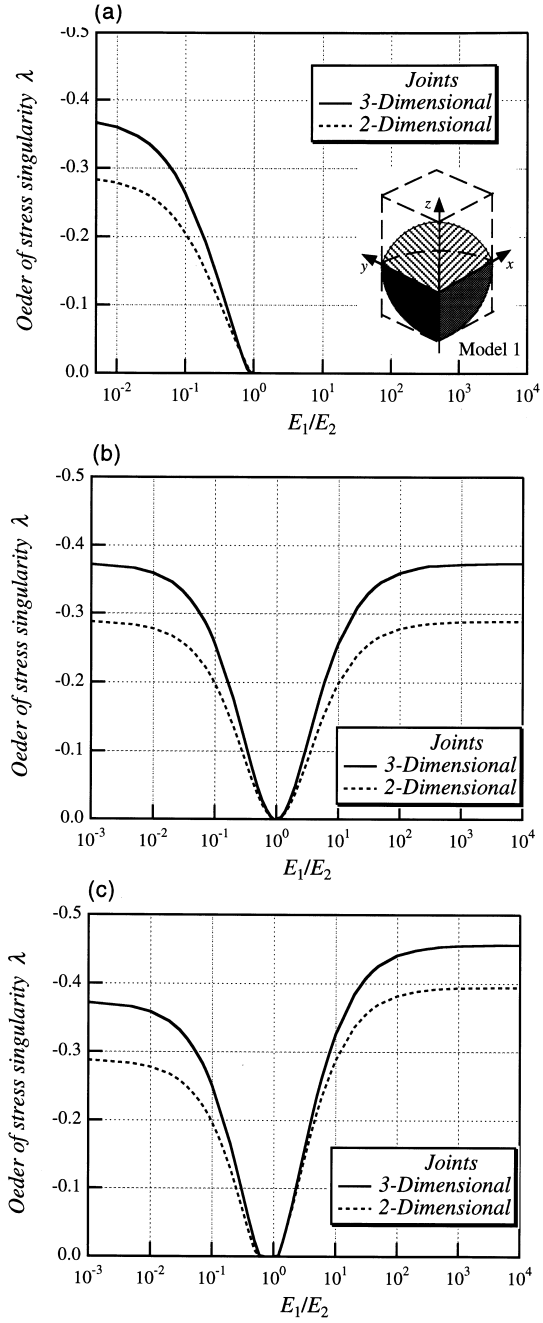

Fig. 18. Relationship between the order of stress singularity and Young's moduli ratio E_1/E_2 for the 1/8–1/8 joint. Comparison of the order of stress singularity for two-dimensional joints and three-dimensional joints. (a) $\nu_1 = 0.3$, $\nu_2 = 0.0$; (b) $\nu_1 = 0.3$, $\nu_2 = 0.3$; (c) $\nu_1 = 0.3$, $\nu_2 = 0.48$.

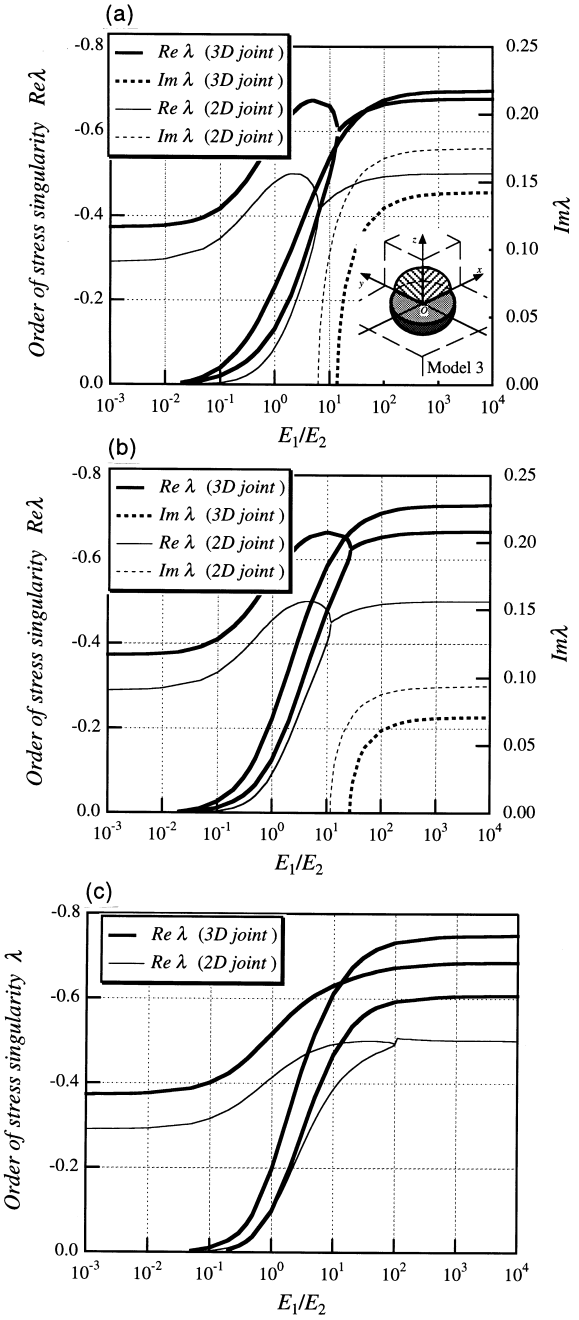

Fig. 19. Relationship between the order of stress singularity and Young's moduli ratio E_1/E_2 for the 1/8–1/2 joint. Comparison of the order of stress singularity for two-dimensional joints and three-dimensional joints. (a) $\nu_1 = 0.3$, $\nu_2 = 0.0$; (b) $\nu_1 = 0.3$, $\nu_2 = 0.3$; (c) $\nu_1 = 0.3$, $\nu_2 = 0.48$.

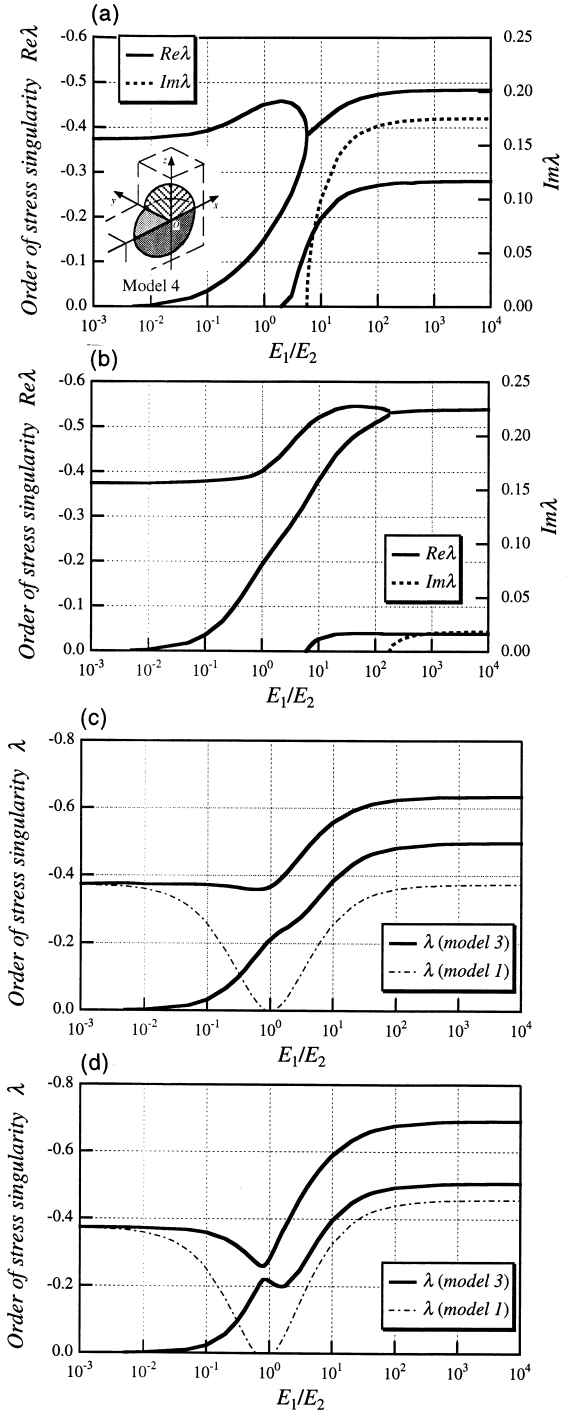

Fig. 20. Relationship between the order of stress singularity and Young's moduli ratio E_1/E_2 for the 1/8–1/4 joint. (a) $\nu_1 = 0.3$, $\nu_2 = 0.0$; (b) $\nu_1 = 0.3$, $\nu_2 = 0.2$; (c) $\nu_1 = 0.3$, $\nu_2 = 0.3$; (d) $\nu_1 = 0.3$, $\nu_2 = 0.48$.

order of singularity exist over the whole range of E_1/E_2 in our calculation and the largest value of the order of stress singularity is about -0.75.

The order of singularity for model 4 is shown against E_1/E_2 for $\nu_2 = 0.0$, 0.2, 0.3, and 0.48 in Fig. 20. The order of singularity for model 1 is also shown in Fig. 20(c) and (d) along with the results for three-dimensional joints. There are no two-dimensional joints corresponding to model 4, since model 4 can be viewed as a joint with a different configuration depending on the directional perspective. In the case of a small value of ν_2, three real roots and one complex root yielding singularity exist. As the value of ν_2 increases, the imaginary value and the real values of the order of singularity for a complex root decrease. The number of roots yielding singularity is two in the case of $\nu_2 = 0.3$. In the case of $\nu_2 = 0.48$, Fig. 20(d) shows that the order of singularity fluctuates in an oscillatory manner around $E_1/E_2 = 1$. This distinct variation can be explained by the difference in Poisson's ratio as follows. When Poisson's ratio of material 2 is small, region 2 shrinks little and expands by the force applied by region 1; thus it behaves like a semi-elastic region compared to region 1. On the contrary, when ν_2 increases, region 2 expands and shrinks in the bonded plane by force acting on it from region 1, and behaves like the one in model 1. Hence, in the case of a large E_1/E_2, i.e. small value of E_2, the above-mentioned things become noticeable. A complicated variation of the order of singularity around $E_1/E_2 = 1$ with large ν_2 must be attributed to the disappearance of the stress singularity in model 1.

When two stress singularity lines with different values of order meet as in model 4, the order of singularity varies against E_1/E_2 in a manner similar to model 3 with $\nu_2 < 0.3$ and model 1 with $\nu_2 > 0.3$. The order of singularity for model 1 and 3 varies against E_1/E_2 in a manner similar to two-dimensional joints with the cross section of three-dimensional joints. That is to say, the order of singularity at a vertex where two stress singularity lines with different values of order meet is influenced largely by either stress singularity line depending on the material combination of joints.

5. Conclusion

We investigated the order of singularity at the vertex of three-dimensional dissimilar materials using the FEM, taking the stress singularity field into consideration in an interpolation function. In this investigation, Dundurs' parameters, α_{3D}–β_{3D}, in three-dimensional stress states were introduced, and contour maps of the order of singularity for two- and three-dimensional joints were mapped on a α_{3D}–β_{3D} plane and an ordinary α_{2D}–β_{2D} plane. As a result of the comparison of the order of singularity for three-dimensional joints and two-dimensional joints on the same plane, the order of singularity in three-dimensional joints is larger than that in two-dimensional joints, when the values of α_{2D} and β_{2D} are fixed. However, the zero-boundary of stress singularity in both joints is almost identical. When the loci of the order of singularity were mapped on the α_{3D}–β_{3D} plane, the zero-boundary of singularity was almost independent of Poisson's ratio, although the loci of the order of singularity depended slightly on Poisson's ratio, except at the zero-boundary. The order of singularity was affected also by the variation of the vertex angle between two free side-surfaces. The values of the order of stress singularity obtained by solving an eigenequation based on a FEM formulation are fairly agreed with those obtained from the slope of stress distribution derived using BEM. The order of singularity increases with the decreasing vertex angle. In particular, the influence of the vertex angle upon the order of singularity becomes noticeable in wider vertex angles.

The order of singularity in 1/8–1/4 and 1/8–1/2 joints was examined against E_1/E_2 at several values of Poisson's ratio. In smaller values of Poisson's ratio of material 2, a complex root yielding a singularity occurred in both joints. At larger values of Poisson's ratio of material 2, two or three real roots yielding the order of singularity are generated. In particular, in the case of 1/8–1/4 joint, the order of singularity fluctuated in an oscillatory manner around $E_1/E_2 = 1$, and it became similar to the behavior of

singularity of 1/8–1/8 joint in the range of $E_1/E_2 > 1$. The order of singularity at the vertex where two stress singularity lines with different orders meet is affected significantly by either of the stress singularity lines depending on the configuration of the side surfaces and the material combinations.

Acknowledgements

I thank Professor Masataka Kobayashi at Nagaoka Technical College and Ikuo Ihara at Nagaoka University of Technology for their valuable suggestions and discussion.

References

Barsoum, R.S., 1988. Theoretical basis of the finite element iterative method for the eigenvalue problem in stationary cracks. Int. J. Numer. Methods Eng. 26, 531–539.

Bazant, Z.P., 1974. Three-dimensional harmonic functions near termination or intesection of gradient singularity lines: a general numerical method. Int. J. Engng Sci. 12, 221–243.

Bazant, Z.P., Estenssoro, L.F., 1979. Surface singularity and crack propagation. Int. J. Solid Structures 15, 405–426.

Bazant, Z.P., Kerr, L.M., 1974. Singularities of elastic stresses and of harmonic functions at conical notches and inclusions. Int. J. Solids Struct. 10, 957–964.

Benthem, J.P., 1977. State of stress at the vertex of a quarter-infinite crack in a half-space. Int. J. Solid Structures 13, 479–491.

Benthem, J.P., 1980. The quarter-infinite crack in a half space; alternative and additional solutions. Int. J. Solid Structures 16, 119–130.

Bogy, D.B., 1968. Edge-bonded dissimilar orthogonal elastic wedges under normal and shear loading. J. Appl. Mech. 35, 460–466.

Bogy, D.B., 1970. On the problem of edge-bonded elastic quarter-planes at the boundary. Int. J. Solids and Struct. 6, 1287–1313.

Bogy, D.B., 1971a. Two-edge bonded elastic wedges of different materials and wedge angles under surface tractions-2. J. Appl. Mech. 38 (2), 377–386.

Bogy, D.B., 1971b. On the plane elastostatic problem of a loaded crack terminating at a material interface. J. Appl. Mech. 38, 911–918.

Cook, T.S., Erdogan, F., 1972. Stresses in bonded materials with a crack perpendicular to the interface. Int. J. Engng Sci. 10, 677–697.

Dempsey, J.P., Sinclair, G.B., 1979. On the stress singularities in the plane elasticity of the composite wedge. J. Elasticity 9 (4), 373–391.

Dundurs, J., 1969. Discussion of edge-bonded dissimilar orthogonal elastic wedges under normal and shear loading. J. Appl. Mech. 36, 650–652.

Fenner, D.N., 1976. Stress singularities in composite materials with an arbitrarily oriented crack meeting an interface. Int. J. Fracture 12 (5), 705–721.

Ghahremani, F., Hutchinson, J.W., Tvergaard, V., 1990. Three-dimensional effects in microcrack nucleation in brittle polycrystals. J. Am. Ceram. Soc. 73 (6), 1548–1554.

Ghahremani, F., 1991. Numerical variational method for extracting 3D singularities. Int. J. Solids and Structures 27, 1371–1386.

Ghahremani, F., Shih, C.F., 1992. Corner singularity of three-dimensional planar interface cracks. J. Appl. Mech. 59, 61–68.

Hein, V.L., Erdogan, F., 1971. Stress singularities in a two-material wedge. Int. J. Fracture Mechanics 7 (3), 317–330.

Kerr, L.M., Parihar, K.S., 1977. Singularity at the vertex of pyramidal notches with three equal angles. Q. J. Appl. Math. 35, 401–405.

Kerr, L.M., Parihar, K.S., 1978. Elastic stress singularities at conical inclusions. Int. J. Solids Struct. 14, 261–263.

Koguchi, H., Hino, T., Kikuchi, Y., Yada, T., 1994. Residual stress analysis of joints of ceramics and metals. Experimental Mechanics 34, 116–124.

Koguchi, H., Inoue, T., Yada, T., 1995. Stress singularity in three-phase bonded structure. J. Appl. Mech. 63, 252–258.

Li, Y., Koguchi, H., Yada, T., 1992. Investigation of method of stress relaxation around the apex of ceramics-metal bonded structure (consideration of shape effect of apex in three dimensional dissimilar materials). Trans. Jpn. Soc. Mech. Eng. 58, 1417–1423.

Koguchi, H., 1997. Singularity analysis in three-dimensional bonded structure. Int. J. Solids Structures 34 (4), 461–480.

Nakamura, T., Parks, D.M., 1988. Three-dimensional stress field near the crack front of a thin elastic plate. J. Appl. Mech. 55, 805–813.

Pageau, S.S., Joseph, P.F., Biggers, S.B., 1994. The order of stress singularities for bonded and disbonded three-material junctions. Int. J. Solids and Struct. 31, 2979–2997.

Pageau, S.S., Biggers Jr, S.B., 1995. Finite element evaluation of free-edge singular stress fields in anisotropic materials. Int. J. Num. Method in Engineering 38, 2225–2239.

Picu, C.R., Gupta, V., 1997. Three-dimensional stress singularities at the tip of a grain triple junction line intersecting the free surface. J. Mech. Phys. Solids 45 (9), 1495–1520.

Rongved, L., 1955. Force interior to one of two joined semi-infinite solids. Second midwestern conference on solid mechanics. 1–13.

Somaratna, N., Ting, T.C., 1986. Three-dimensional stress singularities in anisotropic materials and composites. Int. J. Eng. Science 24, 1115–1134.

Theocaris, P.S., 1974. The order of singularity at a multi-wedge corner of a composite plate. Int. J. Eng. Science 12, 107–120.

Yamada, Y., Okumura, H., 1981. Analysis of local stress in composite materials by the 3-D finite element. In: Proceedings of the Japan–U.S. Conference, Tokyo, pp. 55–64.

Yang, Y.Y., Munz, D., 1994. Determination of the regular stress term in a dissimilar materials joint under thermal loading by the Mellin transform. J. Thermal Stresses 17, 321–336.